Progress In Electromagnetics Research M, Vol. 81, 43–54, 2019

A Novel Method for ISAR Imaging of Multiple Maneuvering Targets

Jia Zhao[1, *], Yunqi Zhang[1], Xin Wang[2], Sheng Wang[1], and Feng Shang[1]

Abstract—For inverse synthetic aperture radar (ISAR) imaging of multiple targets, range profiles of different targets are sometimes coupled together, resulting in the ineffectiveness of traditional imaging method, while the couplings in range domain may behave differently in time-frequency domain, and the Doppler histories of different targets are potentially separable. Then the time-frequency analysis method can be utilized for signal separation of multiple targets. Notice that the nonuniform motions of targets may make the time-frequency curves changeful, and accordingly some preprocessing are needed. In this paper, a novel ISAR imaging method based on modified keystone transform (MKT), short-time Fourier transform (STFT), and Hough transform (HT) is proposed. The radar echoes of multiple targets are approximated to a second-order polynomial. The MKT is firstly utilized to correct the range curvatures. Secondly, the signal in each range cell is transformed into time-frequency domain through the STFT. Meanwhile, HT theory and mask matrix are adopted in time-frequency curves' separation of different targets. Thirdly, after inverse STFT, the separated time-frequency curves are respectively back to the range domain, and the range profiles of different targets are successfully separated. Eventually, with further motion compensation and precise imaging, focused ISAR images of different targets are achieved. Simulation results demonstrate the validity of the proposed method.

1. INTRODUCTION

Inverse synthetic aperture radar (ISAR) imaging is an efficient method for providing high resolution images of maneuvering targets especially in many military applications such as target identification, recognition, and classification. Parameter estimation and motion compensation are the key issues of ISAR imaging [1–6]. In modern warfare, intensive multiple targets are often present in radar line-of-sight in various applications such as aircraft or ship formation, ballistic missile with multiple warheads, and space debris, which pose a challenge to the existing imaging techniques [7–9].

In the same radar antenna beam, multiple targets may share analogous translational motion or behave variously. Various approaches have been proposed for ISAR imaging of multiple targets. In the first case, coarse imaging results of multiple targets are obtained via traditional single target imaging methods, and then different targets could be extracted via image segmentation and accurate imaging. In the second case, the traditional single target imaging methods may perform poorly. Within a short time of observation, the motion of targets can usually be reviewed as uniformly accelerated motion. The Doppler frequency produced by the translational motion of the target is a linear frequency modulated (LFM) signal, and the chirp rate is proportional to the acceleration of the target. Hence, multiple targets could be segmented and extracted via different parameters [10–12]. Some methods segment the signals of different targets into bulk images and invert them to obtain equivalent raw data [13–15]. Such raw data are then the input to an ISAR processor that aims at forming well-focused ISAR images. Several line or curve detection based methods directly separate the range profiles of different targets, such as

Received 23 January 2019, Accepted 10 April 2019, Scheduled 6 May 2019
* Corresponding author: Jia Zhao (jiazhao0216@gmail.com).
[1] School of Electronic Engineering, XI'AN University of Posts & Telecommunications, Xi'an, China. [2] SWIEE International, Southwest China Research Institute of Electronic Equipment, Chengdu, China.

the Hough transform (HT) [16] for line detection and the particle swarm optimization (PSO) [13, 17] for curve estimation. In general, convictive results could be obtained when the range profiles of different targets are apparently distinguishable. However, when the range profiles of different targets are coupled seriously, performances of some methods would degrade. It is found that the couplings in range domain may behave differently in time-frequency domain, that is, the Doppler histories of different targets may be potentially separable.

In this paper, a novel ISAR imaging method based on modified keystone transform (MKT), short-time Fourier transform (STFT), and HT is proposed for multiple targets. KT is a popular motion compensation method in SAR/ISAR [18, 19]. By transforming a slow time variable to a virtual slow time variable, it can achieve arbitrary linear range migration correction without the prior information of the target. However, when the target exhibits nonuniform motion, that is, radial and angular acceleration, acceleration rate, etc., the original KT becomes invalid. Hence, various MKT methods are developed with more attentions on single target [20–22]. In our case, the radar echoes of multiple targets are approximated to a second-order polynomial. The MKT is first employed to correct the range curvatures. Then the signal in each range cell is transformed into time-frequency domain through the STFT, and the slopes of different time-frequency curves are detected by the HT [16]. Based on this, the mask matrixes are constructed, and time-frequency curves' separation is performed. After that, by means of inverse STFT, the separated time-frequency curves are respectively back to the range domain, and the range profiles of different targets are successfully separated. At this point, precise compensation could be carried out for each target. Eventually, focused ISAR images of different targets are obtained.

The organization of this paper is as follows. In Section 2, the ISAR imaging model of multiple targets is established. Then, the MKT, STFT, and HT based ISAR imaging method is proposed in Section 3. In Section 4, simulation results are presented. Finally, Section 5 concludes this paper briefly.

2. ISAR IMAGING MODEL

The geometry for ISAR imaging of multiple targets is shown in Figure 1. The instant distance between the radar and the targets can be expressed as

$$R_{ij}(t_m) = R_{i0} + v_{ir}t_m + \frac{1}{2}a_{ir}t_m^2 + x_{ij}\cos(\omega_i t_m) + y_{ij}\sin(\omega_i t_m) \tag{1}$$

where the corner marks i and j represent the j_{th} scatterer on the i_{th} target. R_{i0} is the initial distance between the radar and the i_{th} target. v_{ir} and a_{ir} are the radial velocity and acceleration, respectively. t_m refers to the slow time variable. x_{ij} and y_{ij} are the coordinates of the j_{th} scatterer on the i_{th} target. ω_i is the angular velocity.

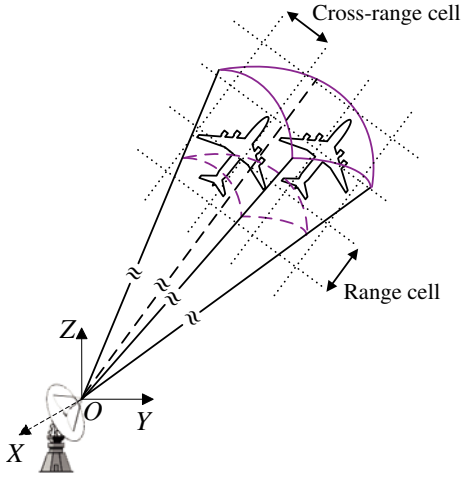

Figure 1. ISAR imaging geometry of multiple targets.

In practice, the rotation angle of the target during the coherent processing interval (CPI) is usually small, thus approximations $\cos(\omega_i t_m) \approx 1$ and $\sin(\omega_i t_m) \approx \omega_i t_m$ can be tolerated. Then, Equation (1) is denoted as

$$R_{ij}(t_m) = R_{i0} + x_{ij} + (v_{ir} + y_{ij}\omega_i)t_m + \frac{1}{2}a_{ir}t_m^2. \tag{2}$$

Suppose that the radar transmits LFM signal, which is given as

$$u(t) = rect(t/T_p)\exp(j\pi k t^2) \tag{3}$$

where T_p is the pulse width, $k = B/T_p$ the chirp rate, and B the bandwidth. Assuming that the radar emits N pulses during the CPI, the received signals can be written as

$$s(\tilde{t}, t_m) = \sum_i \sum_j A_{ij} u(\tilde{t} - 2R_{ij}(t_m)/c) \exp\left(-j\frac{4\pi f_c}{c} R_{ij}(t_m)\right) \tag{4}$$

where A_{ij} is the amplitude of the j_{th} scatterer on the i_{th} target, $\tilde{t} = t - nT_r$ the fast time, $n = 1, \cdots, N$, T_r the pulse repetition interval (PRI), and f_c the center frequency of the radar.

According to the principle of stationary phase [23], the Fourier transform of $u(\tilde{t})$ is

$$U(f) = \frac{1}{\sqrt{k}} rect\left(\frac{f}{B}\right) \exp\left(-j\frac{\pi f^2}{k}\right) \tag{5}$$

Then the Fourier transform of Equation (4) over the fast time $\tilde{t}$ is

$$S(f, t_m) = \sum_i \sum_j A_{ij} U(f) \exp\left[-j\frac{4\pi(f + f_c)}{c} R_{ij}(t_m)\right] \tag{6}$$

After matched filter, we obtain

$$Y(f, t_m) = \sum_i \sum_j A_{ij} \left|U(f)\right|^2 \exp\left[-j\frac{4\pi(f + f_c)}{c} R_{ij}(t_m)\right] \tag{7}$$

where f is the range frequency vector. According to Equation (7), we know that the range migrations arise from the coupling between f and t_m, i.e., the exponential term in Equation (7).

3. PROPOSED METHOD

Signal separation is a direct method for ISAR imaging of multiple targets. For multiple targets in the same radar antenna beam, the range profiles of different targets might present two kinds of situations: distinguishable or coupled. In case 1, it is easy to implement. However, in case 2, coarse separation in range domain may lead to undesirable results. When range curvatures exist, the situation becomes more complicated.

While the couplings in range domain may behave differently in time-frequency domain, and the Doppler histories of different targets are potentially separable. Considering that the possible range curvatures may make a difference on the separation in time-frequency domain, range curvatures correction should be carried out in advance.

The original KT decouples f and t_m by transforming t_m in the slow time domain to τ_m in the virtual slow time domain as [18, 24]

$$t_m = \frac{f_c}{f + f_c}\tau_m. \tag{8}$$

The original discrete data in the ($f \sim t_m$) plane and the data after KT in the ($f \sim \tau_m$) plane are compared in Figure 2, with the hollow and solid points representing the original data and the reformatting data, respectively. By this way, the KT can achieve arbitrary linear range migration correction without the prior information of the target. When the target exhibits uniform motion, the original KT can function effectively. However, when the target exhibits nonuniform motion, that is, accompanied by acceleration, acceleration rate, etc., the radar echo is approximated to second-order or

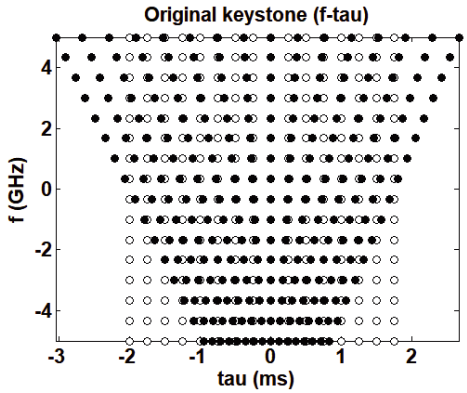

Figure 2. Data reformatting comparison after original KT.

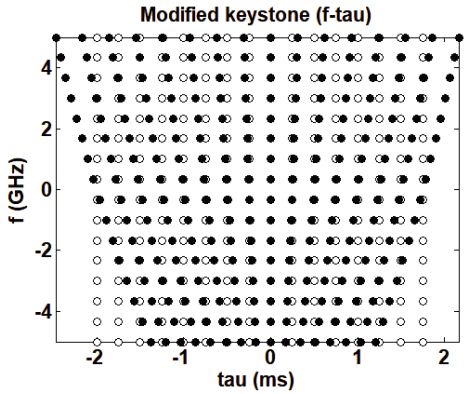

Figure 3. Data reformatting comparison after MKT.

high-order polynomial. At this point, the original KT becomes invalid. Then, different MKT methods are developed. In our case, the radar echoes of multiple targets are approximated to a second-order polynomial, and the corresponding MKT can be written as

$$t_m = \left(\frac{f_c}{f+f_c}\right)^{1/2} \tau_m. \tag{9}$$

Similar data reformatting comparison is shown in Figure 3. It is seen that after the original KT, the data show an isosceles trapezoid. While after the MKT, it is no longer isosceles trapezoid, and the left and right borders manifest as parabolas, which are $y = x^{1/2}$ and $y = x^{-1/2}$ [25]. By taking Equation (9) into Equation (7), we obtain

$$\begin{aligned} Y(f,t_m) \;=\; & \sum_i \sum_j A_{ij} \left|U(f)\right|^2 \exp\left[-j\frac{4\pi(f+f_c)}{c}(R_{i0}+x_{ij})\right] \\ & \cdot \exp\left[-j\frac{4\pi\sqrt{f_c(f+f_c)}}{c}(v_{ir}+y_{ij}\omega_i)\tau_m\right] \exp\left[-j\frac{2\pi f_c}{c}a_{ir}\tau_m^2\right] \end{aligned} \tag{10}$$

It is found that the coupling between f and quadratic term of t_m is eliminated.

After preliminary corrections of range curvatures, time-frequency curves separation in time-frequency domain can be carried out. In simple terms, the processing procedure consists of the following parts: forward transform (range domain to time-frequency domain), lines detection, masks construction, time-frequency curves separation, and inverse transform (time-frequency domain to range domain). The main purpose of time-frequency analysis is to provide conveniences for separation of different time-frequency curves, rather than parameter estimation. Then in the selection of time-frequency analysis

method, we give more considerations on avoiding cross-term interference with less consideration on high Doppler resolution. STFT and Wigner-Ville distribution (WVD) are both common time-frequency analysis methods. The STFT and WVD of time-domain signal $x(t)$ are

$$STFT_x(t,\omega) = \int_{-\infty}^{\infty} x(\tau)h(\tau - t)\exp(-j\omega\tau)d\tau \tag{11}$$

and

$$WVD_x(t,\omega) = \int_{-\infty}^{\infty} x\left(t + \frac{\tau}{2}\right)x^*\left(t - \frac{\tau}{2}\right)\exp(-j\omega\tau)d\tau \tag{12}$$

respectively, where $h(t)$ is a rectangle window function.

In the case of multi-component signal, that is, $x(t) = x_1(t) + x_2(t) + \ldots$, the STFT exhibits a little lower resolution while producing no cross-term, and the WVD can provide higher resolution while suffering from cross-term interference. Whether forward transform or inverse transform, the WVD generates larger amounts of computation than the STFT. Therefore, we choose STFT to implement the domain transformation under multi-component signal circumstances.

After transforming from range domain to time-frequency domain, Doppler histories of different targets are revealed. The couplings in range domain may be potentially separable in time-frequency domain, and the Doppler histories of different targets manifest as "diagonal stripes" with different slopes. Accordingly, HT is utilized for time-frequency curves separation of different targets.

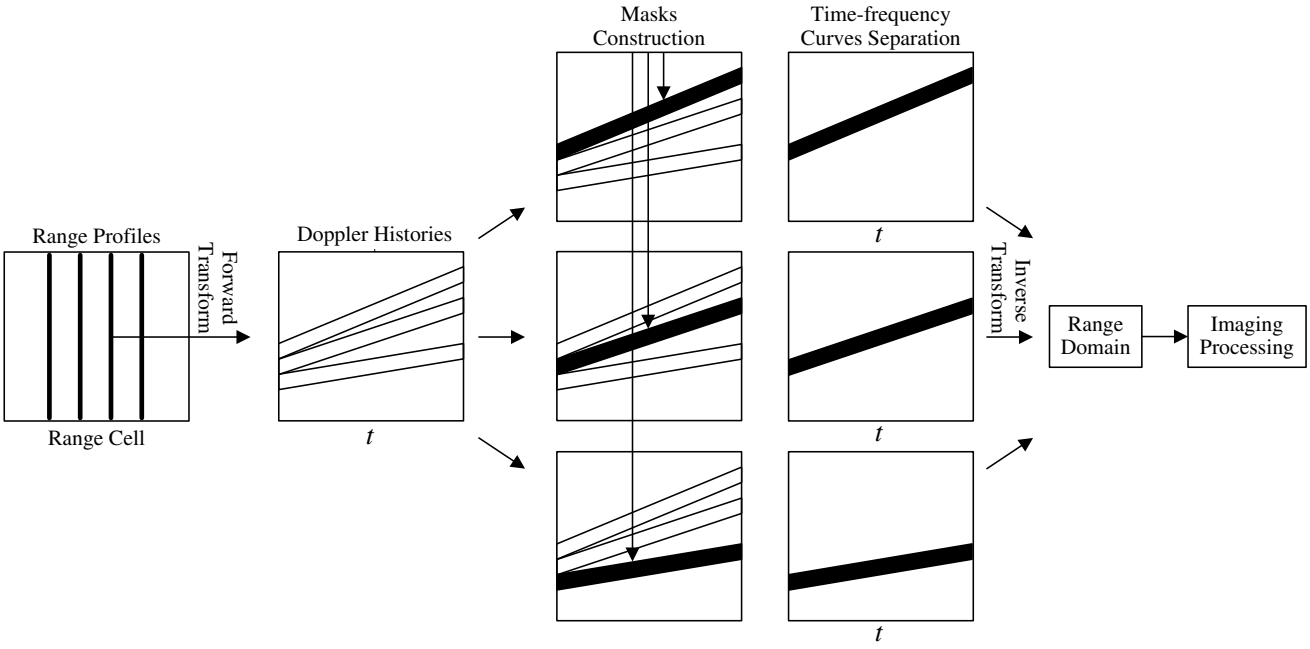

Figure 4. Flow diagram of time-frequency curves separation.

In conjunction with the flow diagram in Figure 4, the proposed method can be briefly described in eight steps below.

Step 1 Match filtering of the radar echo signal.

Step 2 Apply the MKT to realize range curvatures correction.

Step 3 Take any of the range cells, and transform the data from range domain to time-frequency domain by forward STFT.

Step 4 Employ the HT to detect different "diagonal stripes", and construct masks.

Step 5 Utilize the masks to separate different time-frequency curves.

Step 6 Transform the separated data from time-frequency domain to range domain by inverse STFT, respectively. At this point, the radar echo signals of different targets within the range cell are separated.

Step 7 Repeat steps 3, 5, and 6 for all range cells. After this, the whole radar echo signals of each single target are obtained.

Step 8 Perform further precise imaging for each single target.

During the procedure, data in each range cell correspond to a time-frequency image. Then a series of time-frequency images are obtained. It is found that the time-frequency curves corresponding to the same target keep similar slopes and initial frequency in different time-frequency images, although there are some differences in the details. Under this premise, the time-frequency curves separation in different time-frequency images can be carried out with the same masks. This point will be proved in the subsequent simulations.

4. SIMULATION RESULTS

To verify the performance of the proposed method, two targets with different location coordinates and motion parameters are simulated in this section. The targets are assumed to consist of a set of ideal points and have equal scattering magnitude, as illustrated in Figure 5. Their motion parameters are listed in Table 1. The radar is assumed operating at 12 GHz and transmits 384 modulated pulses in each of 600 bursts, with the bandwidth being 200 MHz. The PRF is 500 Hz, and the pulse duration is 3 μs.

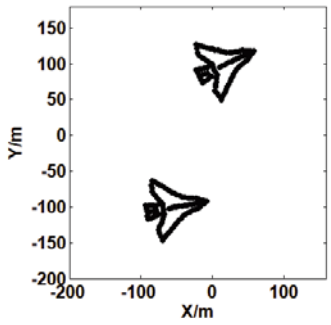

Figure 5. The geometry of two targets.

Table 1. Motion parameters of two targets.

Parameter (units)	Target 1	Target 2
Radial Velocity v_i (m/s)	180	300
Acceleration a_i (m/s^2)	28	29
Angular Velocity ω_i (rad/s)	0.01	0.01

In Figure 6(a), the original range profiles of two targets are displayed, which are partially coupled. On account of the accelerated motion, the range profiles of two targets both show range curvatures to some extent. By employing MKT, the range curvatures are preliminarily corrected, as shown in Figure 6(b).

Freely choosing four different range cells data and taking STFT, we yield Figure 7. It is observed that the Doppler histories of different targets are distinguishable, and the time-frequency curves corresponding to the same target keep similar slopes and initial frequency in different time-frequency images. Hence, the time-frequency curves separation in different time-frequency images can be carried out with the same masks.

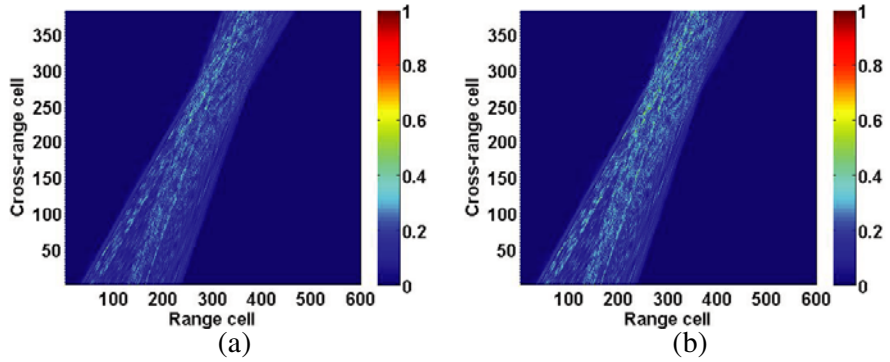

Figure 6. The range profiles of two targets. (a) the original range profiles. (b) the range profiles after MKT.

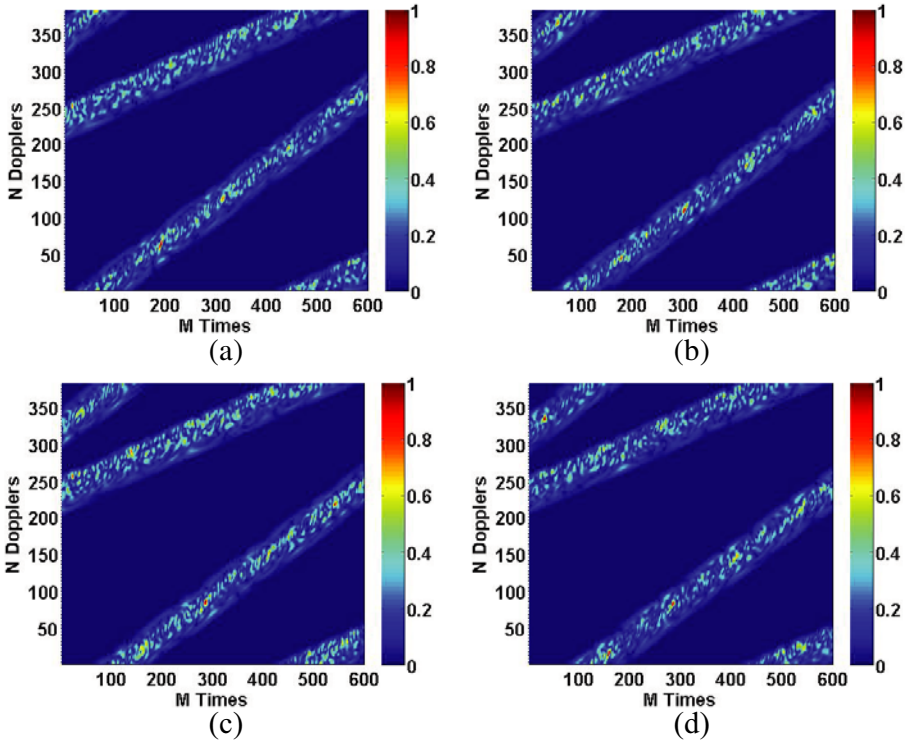

Figure 7. STFT of four different range cells data (with MKT). (a) 80th. (b) 170th. (c) 290th. (d) 330th.

In Figure 8, STFTs of four different range cells data are drawn again. Unlike the results in Figure 7, MKT is not imported, and the range cells data are directly from matching filtering results. As one can see, the time-frequency images are cluttered, and the time-frequency curves corresponding to different targets are undistinguishable. This illustrates the necessity of range curvatures correction and the effectiveness of MKT, although the range curvatures are slight in this simulation (comparison of Figure 6(a) and Figure 6(b)).

Through HT, the different diagonal stripes (corresponding to time-frequency curves of different targets) can be detected, and the masks are constructed, as shown in Figure 9. Apply the masks to Figure 7, and the time-frequency curves separation results are obtained, as Figure 10 displays. Repeat this process for all range cells data, and the two targets are completely separated in time-frequency domain. Transform the separated data from time-frequency domain to range domain by inverse STFT,

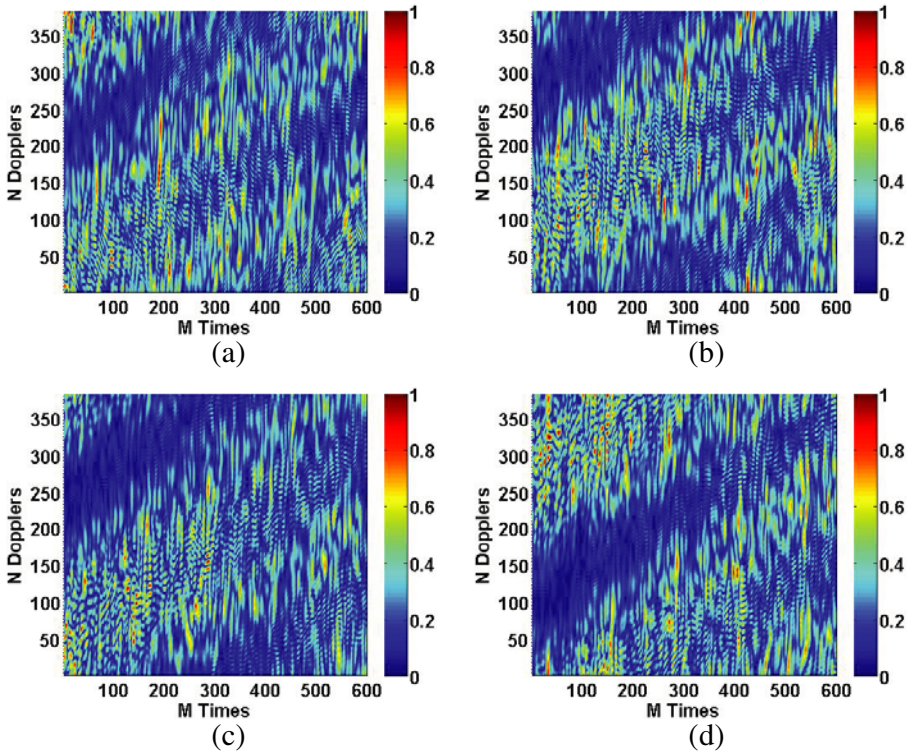

Figure 8. STFT of four different range cells data (without MKT). (a) 80th. (b) 170th. (c) 290th. (d) 330th.

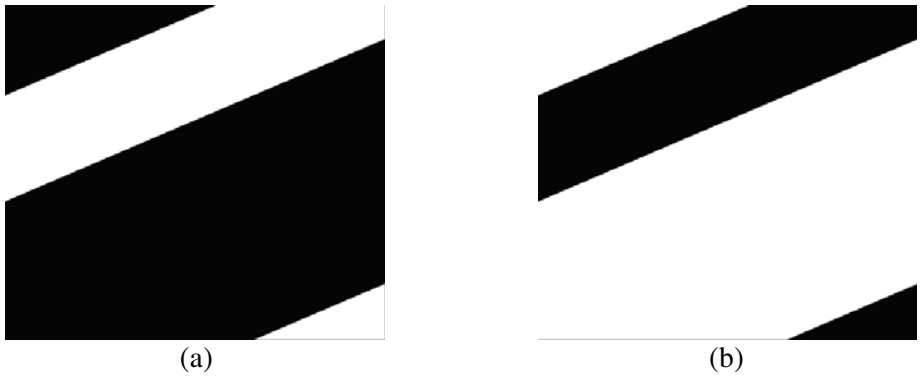

Figure 9. Masks for separation of different time-frequency curves. (a) mask 1. (b) mask 2.

and the partially coupled range profiles of two targets are entirely separated, with the results presented in Figure 11. After that, perform further motion compensation and precise imaging for each single target data. In Figure 12, the ISAR images of two targets using the proposed method are displayed. The results indicate the correctness and effectiveness of the proposed method.

By way of comparison, the method using the HT only (without time-frequency processing) is applied to deal with this case again, and the results are given in Figure 13. To evaluate the image quality, Shannon entropy is adopted here. Suppose that the ISAR image matrix is I, which has M rows and N columns, then the Shannon entropy $\tilde{E}$ is defined as [22, 26]

$$\tilde{E}(I) = -\sum_{m=1}^{M}\sum_{n=1}^{N} I'[m,n] \cdot \ln(I'[m,n]) \tag{13}$$

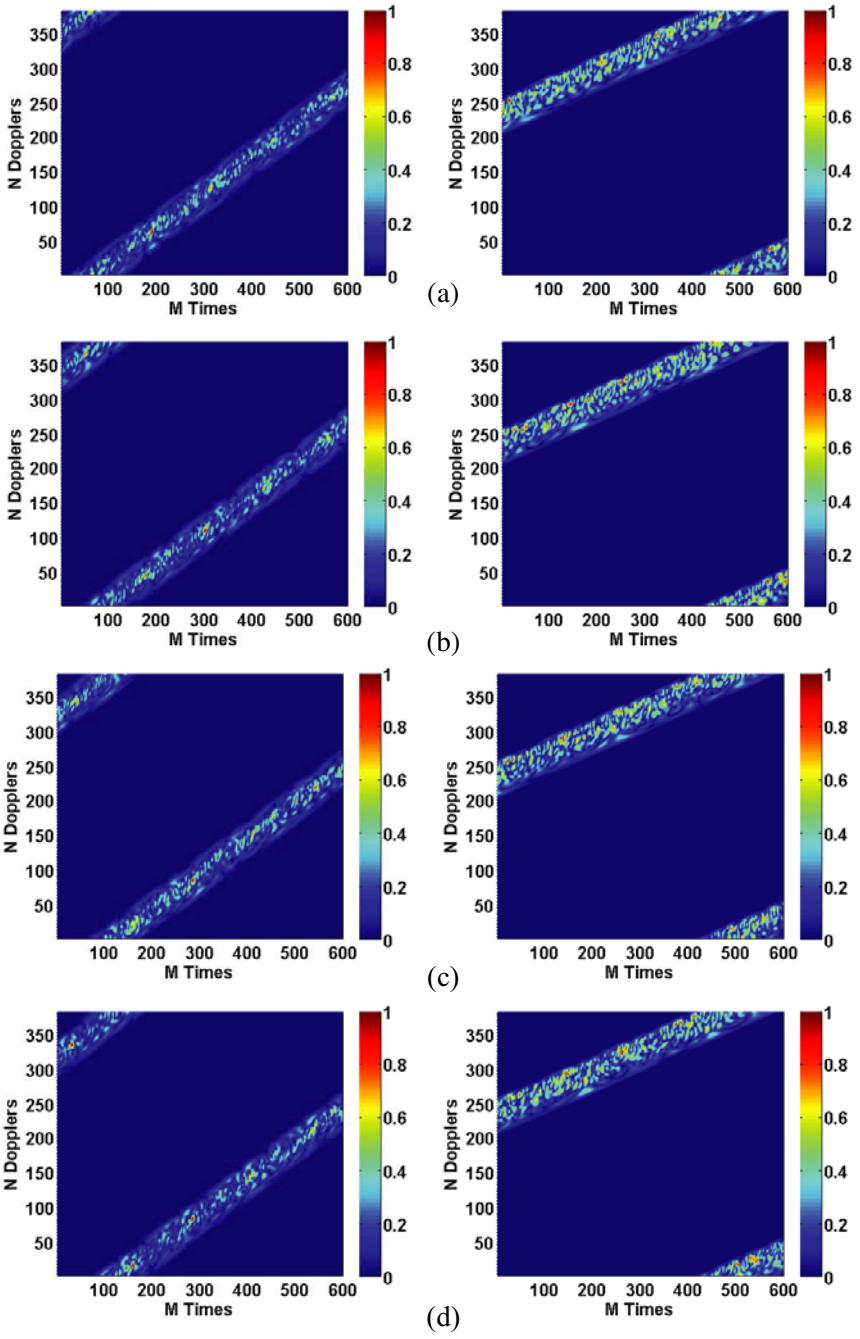

Figure 10. Time-frequency curves separation results of four different range cells data. (a) 80th. (b) 170th. (c) 290th. (d) 330th.

where

$$I'[m,n] = \frac{|I[m,n]|^2}{\sum_{m=1}^{M}\sum_{n=1}^{N}|I[m,n]|^2} \tag{14}$$

The entropies of ISAR images in Figure 12 and Figure 13 are calculated and listed in Table 2, which reveal the better performance of the proposed method than that using the HT only.

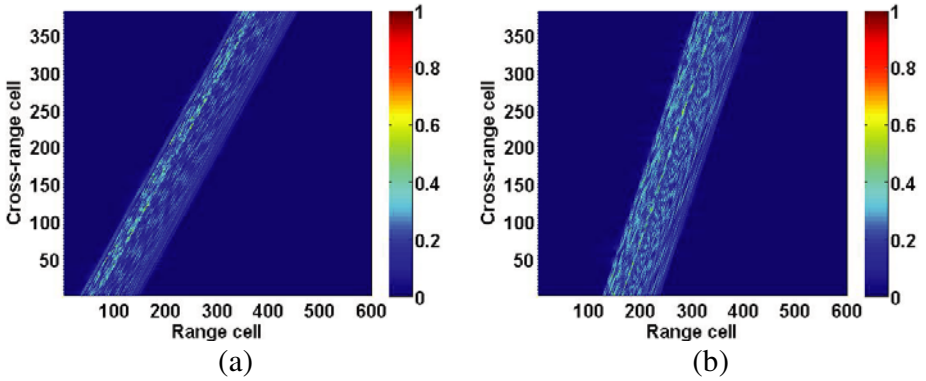

Figure 11. Range profiles separation results of two targets. (a) target 1. (b) target 2.

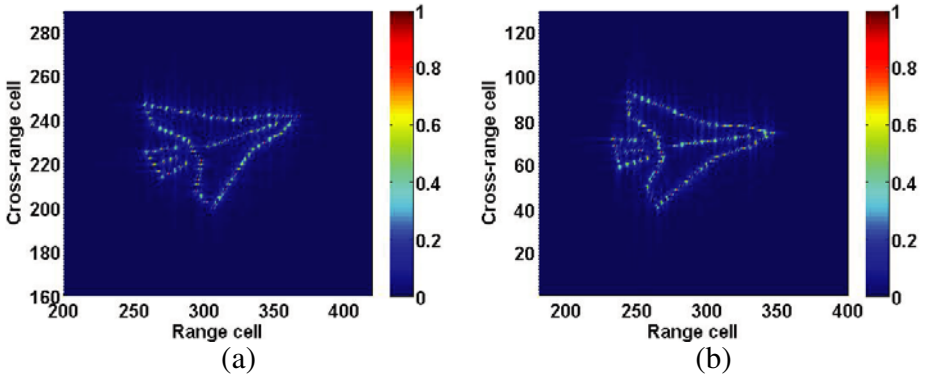

Figure 12. ISAR images of two targets using the proposed method. (a) target 1. (b) target 2.

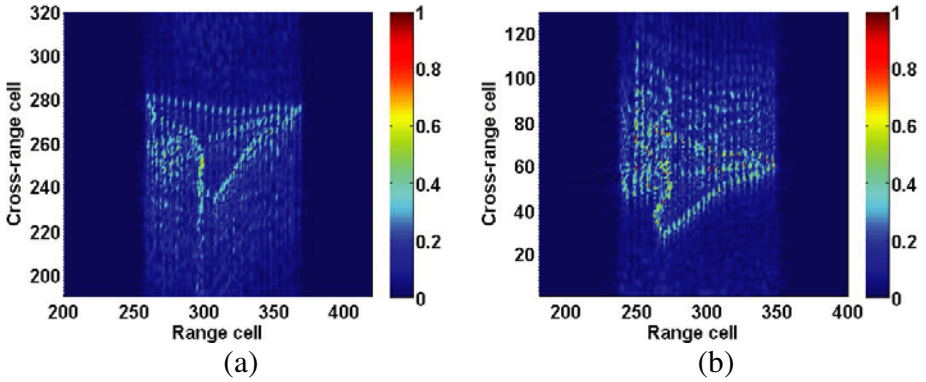

Figure 13. ISAR images of two targets using the HT only (without time-frequency processing). (a) target 1. (b) target 2.

Table 2. Entropies of ISAR images.

Image	Figure 12(a)	Figure 12(b)	Figure 13(a)	Figure 13(b)
Entropy	6.47	6.46	9.63	9.55

5. CONCLUSION

The ISAR imaging of multiple targets is usually more complex than that of single target. In this paper, a novel ISAR imaging method based on MKT, STFT, and HT is proposed. The MKT is utilized for range curvatures correction. STFT and HT are applied to separate the time-frequency curves of different targets. After that, by inverse STFT, the range profile of each single target is obtained. Eventually, with further motion compensation and precise imaging, focused ISAR images of different targets are achieved. Throughout the whole process, the range curvatures correction has a significant impact on the follow-up procedure, and the transformations between range domain and time-frequency domain play an important role in decoupling and lossless separation of multiple targets signals. Simulation and comparison results demonstrate the fine performance of the proposed method.

ACKNOWLEDGMENT

This work was supported in part by the Scientific Research Program Funded by Shaanxi Provincial Education Department (Program No. 18JK0701).

REFERENCES

1. Zheng, J. B., T. Su, W. T. Zhu, and Q. H. Liu, "ISAR imaging of targets with complex motions based on the Keystone time-chirp rate distribution," *IEEE Geoscience and Remote Sensing Letters*, Vol. 11, No. 7, 1275–1279, 2014.
2. Lv, Q., T. Su, and J. Zheng, "Inverse synthetic aperture radar imaging of targets with complex motion based on the local polynomial ambiguity function," *Journal of Applied Remote Sensing*, Vol. 10, No. 1, 015019, 2016.
3. Sun, S. B. and G. Liang, "ISAR imaging of complex motion targets based on Radon transform cubic chirplet decomposition," *International Journal of Remote Sensing*, Vol. 39, No. 6, 1770–1781, 2018.
4. Li, Y. C., M. D. Xing, J. H. Su, Y. H. Quan, and Z. Bao, "A new algorithm of ISAR imaging for maneuvering targets with low SNR," *IEEE Transactions on Aerospace & Electronic Systems*, Vol. 49, No. 1, 543–557, 2013.
5. Qian, J., X. Lv, M. Xing, L. Li, and Z. Bao, "Motion parameter estimation of multiple ground fast-moving targets with a three-channel synthetic aperture radar," *IET Radar, Sonar & Navigation*, Vol. 5, No. 5, 582–592, 2011.
6. Lian, M. and Y. Jiang, "Time-frequency analysis for moving ship targets in GEO spaceborne/airborne bistatic SAR imaging based on a GEO satellite transmitter," *International Journal of Remote Sensing*, Vol. 38, No. 23, 7389–7404, 2017.
7. Li, J., R. Wu, and V. C. Chen, "Robust autofocus algorithm for ISAR imaging of moving targets," *IEEE Transactions on Aerospace and Electronic Systems*, Vol. 37, No. 3, 1056–1069, 2001.
8. Muñoz-Ferreras, J. M., F. Pérez-Martínez, and M. Datcu, "Generalisation of inverse synthetic aperture radar autofocusing methods based on the minimisation of the Renyi entropy," *IET Radar Sonar & Navigation*, Vol. 4, No. 4, 586–594, 2010.
9. Tian, J., W. Cui, X. L. Lv, and S. Wu, "Joint estimation algorithm for multi-targets' motion parameters," *IET Radar Sonar & Navigation*, Vol. 8, No. 8, 939–945, 2014.
10. Li, Y., Y. Fu, X. Li, and L.-W. Li, "ISAR imaging of multiple targets using particle imaging of multiple targets using particle swarm optimisation-adaptive joint time frequency approach," *IET Signal Processing*, Vol. 4, No. 4, 343–351, 2010.
11. Tian, J., W. Cui, and S. Wu, "A novel method for parameter estimation of space moving targets," *IEEE Geoscience & Remote Sensing Letters*, Vol. 11, No. 2, 389–393, 2013.
12. Li, X., G. Cui, W. Yi, and L. Kong, "A fast maneuvering target motion parameters estimation algorithm based on ACCF," *IEEE Signal Processing Letters*, Vol. 22, No. 3, 270–274, 2014.

13. Park, S. H., H. T. Kim, and K. T. Kim, "Segmentation of ISAR images of targets moving in formation," *IEEE Transactions on Geoscience & Remote Sensing*, Vol. 48, No. 4, 2099–2108, 2010.
14. Bai, X. R., F. Zhou, M. D. Xing, and Z. Bao, "A novel method for imaging of group targets moving in a formation," *IEEE Transactions on Geoscience and Remote Sensing*, Vol. 50, No. 1, 221–231, 2012.
15. Martorella, M., E. Giusti, F. Berizzi, A. Bacc, and E. Dalle Mese, "ISAR based techniques for refocusing non-cooperative targets in SAR images," *IET Radar Sonar & Navigation*, Vol. 6, No. 5, 332–340, 2012.
16. Park, S. H., K. K. Park, J. H. Jung, H. T. Kim, and K. T. Kim, "ISAR imaging of multiple targets using edge detection and hough transform," *Journal of Electromagnetic Waves and Applications*, Vol. 22, No. 2–3, 365–373, 2008.
17. Choi, G. G., S. H. Park, H. T. Kim, and K. T. Kim, "ISAR imaging of multiple targets based on particle swarm optimization and hough transform," *Journal of Electromagnetic Waves and Applications*, Vol. 23, No. 14–15, 1825–1834, 2009.
18. Xing, M. D., R. B. Wu, J. Q. Lan, and Z. Bao, "Migration through resolution cell compensation in ISAR imaging," *IEEE Geoscience & Remote Sensing Letters*, Vol. 1, No. 2, 141–144, 2004.
19. Lv, X. L., M. D. Xing, S. H. Zhang, and Z. Bao, "Keystone transformation of the Wigner-Ville distribution for analysis of multicomponent LFM signals," *Signal Processing*, Vol. 89, No. 5, 791–806, 2009.
20. Kirkland, D., "Imaging moving targets using the second-order keystone transform," *IET Radar Sonar & Navigation*, Vol. 5, No. 8, 902–910, 2011.
21. Zhang, J., T. Su, Y. Li, and J. Zheng, "Radar high-speed maneuvering target detection based on joint second-order keystone transform and modified integrated cubic phase function," *Journal of Applied Remote Sensing*, Vol. 10, No. 3, 035009, 2016.
22. Ruan, H., Y. Wu, X. Jia, and W. Ye, "Novel ISAR imaging algorithm for maneuvering targets based on a modified Keystone transform," *IEEE Geoscience & Remote Sensing Letters*, Vol. 11, No. 1, 128–132, 2013.
23. Lin, Q. Q., Z. P. Chen, Y. Zhang, and J. Z. Lin, "Coherent phase compensation method based on direct if sampling in wideband radar," *Progress in Electromagnetics Research*, Vol. 136, 753–764, 2013.
24. Zhu, D. Y., Y. Li, and Z. D. Zhu, "A Keystone transform without interpolation for SAR ground moving-target imaging," *IEEE Geoscience and Remote Sensing Letters*, Vol. 4, No. 1, 18–22, 2007.
25. Zhang, L. and X. H. He, "Approach for airborne radar ISAR imaging of ship target," *IEEE International Conference on Signal Processing*, 2137–2141, 2010.
26. Wang, J., J. Wang, Y. Wu, Y. Zhu, Z. Luo, and Y. Deng, "Phase adjustment for multistatic passive radar imaging based on image entropy and image contrast," *International Journal of Remote Sensing*, Vol. 37, No. 18, 4460–4485, 2016.